ACS APPLIED MATERIALS & INTERFACES
Research Article
www.acsami.org

Understanding the Degradation Mechanism of Lithium Nickel Oxide Cathodes for Li-Ion Batteries

Jing Xu,[†] Enyuan Hu,[‡] Dennis Nordlund,[∥] Apurva Mehta,[∥] Steven N. Ehrlich,[§] Xiao-Qing Yang,[‡] and Wei Tong[*,†]

[†]Energy Storage and Distributed Resources Division, Lawrence Berkeley National Laboratory, Berkeley, California 94720, United States

[‡]Chemistry Division and [§]National Synchrotron Light Source II, Brookhaven National Laboratory, Upton, New York 11973, United States

[∥]Stanford Synchrotron Radiation Lightsource, SLAC National Accelerator Laboratory, Menlo Park, California 94025, United States

ABSTRACT: The phase transition, charge compensation, and local chemical environment of Ni in $LiNiO_2$ were investigated to understand the degradation mechanism. The electrode was subjected to a variety of bulk and surface-sensitive characterization techniques under different charge−discharge cycling conditions. We observed the phase transition from the original hexagonal H1 phase to another two hexagonal phases (H2 and H3) upon Li deintercalation. Moreover, the gradual loss of H3-phase features was revealed during the repeated charges. The reduction in Ni redox activity occurred at both the charge and the discharge states, and it appeared both in the bulk and at the surface over the extended cycles. The degradation of crystal structure significantly contributes to the reduction of Ni redox activity, which in turn causes the cycling performance decay of $LiNiO_2$.

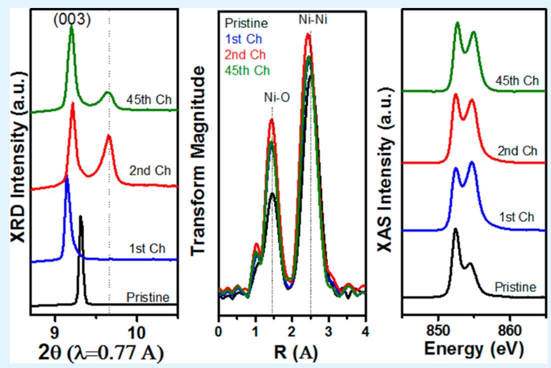

KEYWORDS: *Ni-rich layered oxide cathode, capacity fade, phase evolution, redox reaction, surface characteristics, Li-ion batteries*

■ INTRODUCTION

Rechargeable Li-ion battery technology holds the best promise to serve as power sources for electrical vehicle applications.[1] Of the few cathode material options, layered lithium transition metal oxides ($LiTMO_2$, where TM is a transition metal) are the most promising cathodes for electrical vehicles (EVs) because of their high theoretical capacity (~270 mAh/g) and relatively high average operating voltage (~3.6 V vs Li^+/Li).[2] Continuous searches for better cathodes with higher energy and power density, as well as long cycle life, good safety characteristics, and lower cost, has led to some promising materials, e.g., $LiNi_{1-x-y}Mn_xCo_yO_2$ ($0 < x, y < 1$) (NMC) and $LiNi_{0.8}Co_{0.15}Al_{0.05}O_2$ (NCA).[3,4]

Recently, there is an emerging research interest in achieving even-higher practical capacity by developing Ni-rich layered oxides and charging NMC electrodes to even-higher voltage.[5−8] However, a higher Ni content usually increases the tendency to both surface and bulk phase transformations, particularly at a high state-of-charge or elevated temperature. For example, the highly delithiated $Li_xNi_{0.8}Co_{0.15}Al_{0.05}O_2$ ($x < 0.15$) cathode contains a complex core−shell surface that consists of a layered $R\bar{3}m$ core, a spinel $Fd\bar{3}m$ shell and a rock-salt $Fm\bar{3}m$ structure at the surface.[9] NMC electrodes also suffer from surface instability, particularly under harsh cycling conditions (e.g., high cutoff voltage, 4.7 V).[10−16] This often results from the reduction of transition metals and crystal structural changes (layered $R\bar{3}m$ → rock-salt $Fm\bar{3}m$) at the surface. It ultimately inhibits the kinetics of Li diffusion and increases the cell impedance, leading to a practical capacity loss.[12,13,17] Moreover, such phase transformations also occur when the charged NCA and NMC electrodes are heated. It is initially concomitant with a small amount of oxygen loss followed by an exothermic reaction between oxygen and electrolyte, which further accelerates the decomposition of the cathode and finally facilitates thermal runaway, raising a safety concern.[18] Higher Ni content leads to an even lower onset temperature of the phase transformation and more oxygen release.[18,19]

Despite its obvious advantage in capacity, the major concerns that prevent Ni-rich layered oxides from practical use are cyclability and safety due to surface decomposition and oxygen release, which become more severe at high states-of-charge.[20−27] For NMC and NCA compounds, the presence of several transition metals further complicates the chemical environment at the surface due to the different chemical and electrochemical reactivity of these transition metals, which lead to undesired phase separation and side reactions with the electrolyte.[28,29] Use of $LiNiO_2$, an end member of Ni-rich NMCs and NCA, is of great importance to deconvolute the

Received: September 2, 2016
Accepted: November 1, 2016
Published: November 1, 2016

DOI: 10.1021/acsami.6b11111
ACS Appl. Mater. Interfaces 2016, 8, 31677−31683

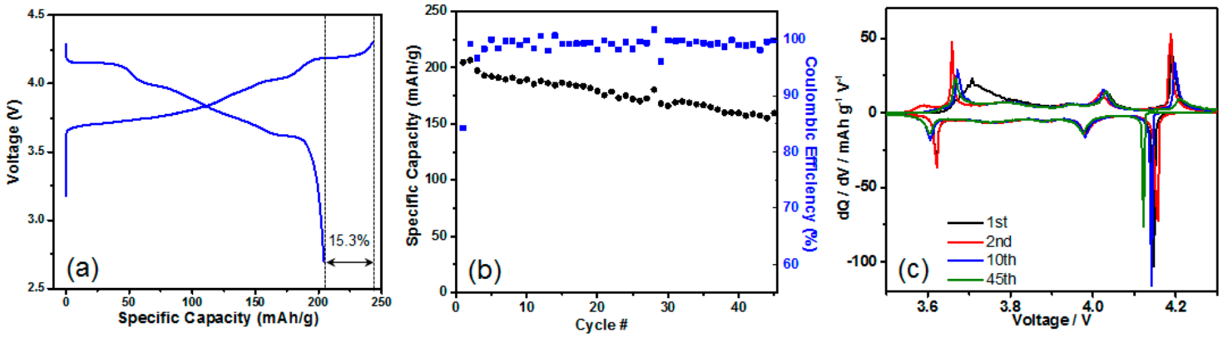

Figure 1. (a) The 1st cycle voltage profiles, (b) cycling performance, and (c) dq/dV plots of $LiNiO_2$. Cells were cycled between 4.3 and 2.7 V (C/10 for cycles 1−2 and C/3 for the subsequent cycles). Capacity at 1 C was defined as 180 mAh/g.

effect of multiple transition metals in NMCs and NCA on the surface and interface properties. Therefore, we investigate $LiNiO_2$ as a model system to reveal the intrinsic performance degradation mechanism originating from high Ni content for those complex $R\bar{3}m$ layered oxides. Previous X-ray diffraction (XRD) studies on $LiNiO_2$ have revealed the phase transformations from the original hexagonal phase (H1) to a second hexagonal (H2) and then to a third hexagonal phase (H3) during the deintercalation process.[30−37] A similar phase transformation and coexistence of two hexagonal phases were also observed at a moderate cutoff voltage (4.4 V) for Ni-rich NMCs and NCA,[38,39] and H3-phase formation occurred when they were charged to higher voltage.[40,41] In addition, the H2-to-H3 phase transformation in $LiNiO_2$ is accompanied by anisotropic lattice changes along the *a*- and *c*-axes, resulting in a large volume change (9%) and inducing microcracks in the $LiNiO_2$ particles when charged above 4.2 V vs Li^+/Li (>0.75 Li deintercalation).[42] X-ray absorption spectroscopy (XAS) studies on $LiNiO_2$ electrode at various states-of-charge have shown: (i) a Jahn−Teller distortion for Ni^{3+}, (ii) electrochemical oxidation of Ni^{3+}, and (iii) an undistorted environment for Ni^{4+}.[43−46] Recently, we found that the surface characteristics of the as-synthesized $LiNiO_2$ (e.g., NiO-like rock-salt species) played a crucial role in the electrochemical performance.[47] However, the majority of the previous work focused on the first cycle behavior of $LiNiO_2$, and few of them tracked the material properties, particularly at the surface, during extended cycling. Therefore, the fundamental degradation mechanism of $LiNiO_2$ cathode needs to be further investigated.

In this work, we report a detailed study on $LiNiO_2$ after different terms of cycling. The phase evolution, charge compensation, and local chemical environment in the bulk and at the surface are characterized as a function of cycle number. These factors simultaneously contribute to the performance decay. This understanding will not only clarify the aging mechanism of $LiNiO_2$ but also shed light on the optimization strategy for Ni-rich layered oxide cathodes in the next generation of Li-ion batteries.

EXPERIMENTAL SECTION

$LiNiO_2$ was prepared by ball-milling Li_2CO_3 (Sigma-Aldrich) and $Ni(OH)_2$ (Sigma-Aldrich) at 500 rpm for 12 h (Retsch, PM100) and then annealing at 750 °C for 12 h under O_2 flow. An extra 10 mol % Li precursor was used to obtain close to stoichiometric $LiNiO_2$.

Electrodes were prepared from slurries containing 80 wt % $LiNiO_2$ active material, 10 wt % polyvinylidene fluoride (PVdF), and 10 wt % acetylene carbon black (Denka, 50% compressed) in *N*-methylpyrrolidone (NMP) solvent. The slurries were cast on carbon-coated aluminum current collectors (Exopack Advanced Coatings) using a doctor blade with the height set to 75 μm and then dried under vacuum at 120 °C overnight to form electrodes. Typical loadings of the active materials were around 2.5 mg/cm^2. Coin cells (2032-type) were assembled in an Ar-filled glovebox (H_2O < 0.1 ppm) with Li metal as the negative electrode. A Celgard 2400 separator and 1 M $LiPF_6$ electrolyte solutions in 1:2 w/w ethylene carbonate and diethyl carbonate (Ferro Corporation) were used to fabricate the cells. Galvanostatic discharge and charge were performed on a Maccor 4200 battery cycler between 4.3 and 2.7 V. Capacity at 1 C was defined as 180 mAh/g. After the cycling of the batteries, the cycled electrodes were washed with dimethyl carbonate three times and dried completely. The cycled electrodes were then encapsulated with polyimide tape inside the glovebox to minimize air exposure for all ex situ experiments. Synchrotron X-ray diffraction (SXRD) data were collected at beamline 7−2 at the Stanford Synchrotron Radiation Lightsource (SSRL) using an incident photon energy of 16.1 keV with the 300k Pilatus area detector. Hard XAS data were collected in transmission mode using a (220) monochromator at SSRL beamline 4−1. Higher harmonics in the X-ray beam were reduced by detuning the Si (220) monochromator. Energy calibration was accomplished by using the first inflection points in the spectra of a Ni reference foil. X-ray absorption near edge spectroscopy (XANES) data were analyzed by Sam's Interface for XAS Package or SIXPACK software, with the photoelectron energy origin E_0 determined by the first inflection point of the absorption edge jump. The soft XAS measurements were carried out on beamline 8−2 at the SSRL and were conducted on powder samples, which were pressed on Au foil to avoid contamination from the adhesive of the carbon tape. Data were acquired under ultrahigh-vacuum (10^{-9} Torr) conditions in a single load at room temperature using total electron yield (TEY) via the drain current and fluorescence yield (FY) modes via a silicon photodiode.

RESULTS AND DISCUSSION

$LiNiO_2$ was synthesized by a conventional solid-state method, the details of which were reported in a previous publication.[47] The as-synthesized $LiNiO_2$ exhibited an initial discharge capacity of 205 mAh/g with a coulombic efficiency of 84.7% during the first cycle (Figure 1a). The discharge capacity showed a slight increase in the second cycle, which could be attributed to better electrolyte wetting or less polarization. However, the capacity gradually degraded in subsequent cycles, and only 160 mAh/g was retained at the end of the 45th cycle, corresponding to 78% of the first cycle capacity (Figure 1b). $LiNiO_2$ experiences a series of phase transformations from the original hexagonal phase (H1) to another hexagonal (H2) and, finally, a third hexagonal phase (H3) upon continuous Li removal during the charge process. These phase transformations are typically reflected by several oxidation−reduction peaks on the differential capacity curves (dq/dV). We observed three distinct oxidation peaks at 3.72, 4.03, and

DOI: 10.1021/acsami.6b11111
ACS Appl. Mater. Interfaces 2016, 8, 31677−31683

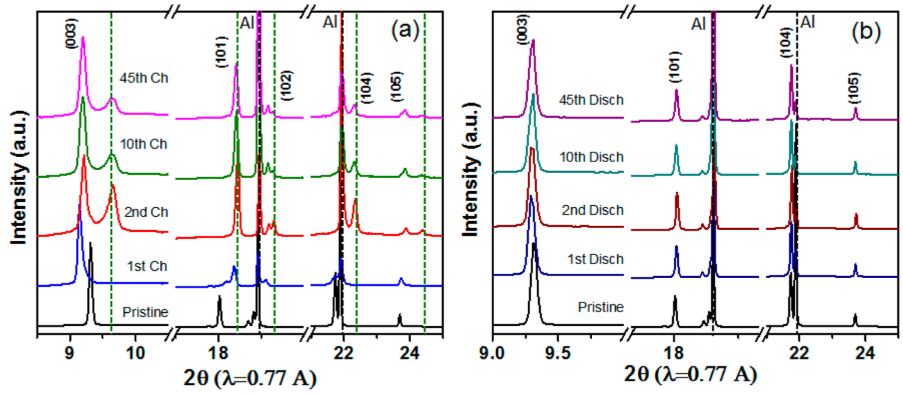

Figure 2. SXRD of $LiNiO_2$ at (a) 4.3 V charge states and (b) 2.7 V discharge states for the selected cycles. Diffraction peaks related to Al current collectors and H3 phases are highlighted by black and green dash lines, respectively.

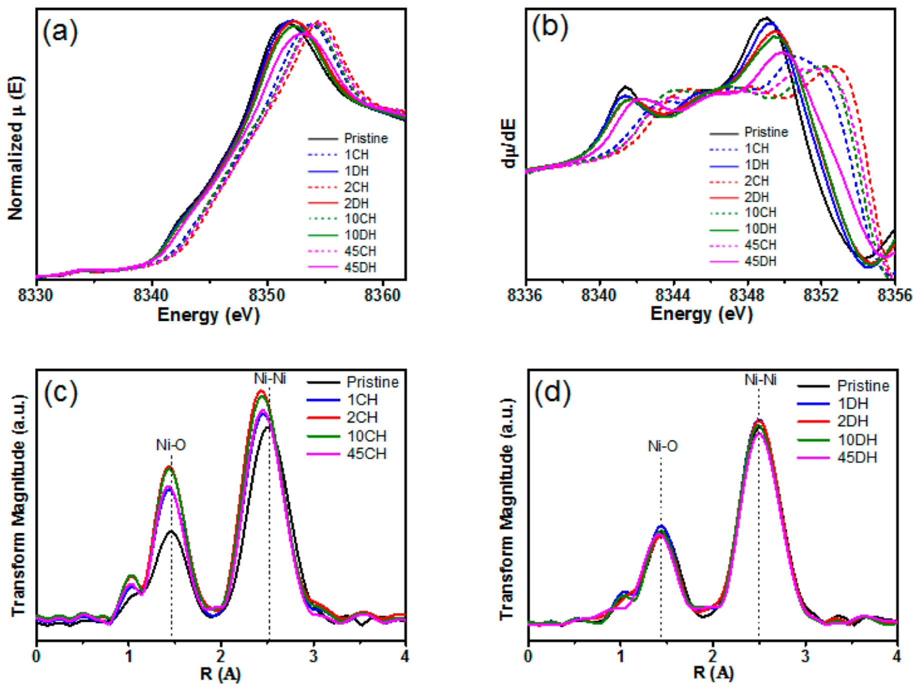

Figure 3. (a) XANES, (b) XANES derivative plots for selected states, and Fourier transform radial distribution function for the Ni K-edge EXAFS at (c) charge and (d) discharge states.

4.19 V during the first charge and their corresponding reduction peaks around 3.61, 3.98, and 4.15 V during the first discharge (black curve in Figure 1c). They can be assigned to the phase transformations from H1 to H2 and H3, respectively.[36,48] After the first cycle, a distinct feature on the dq/dV plot was the shift of the oxidation peak at 3.72 to 3.66 V in the second charge, suggesting a smaller polarization in the second cycle. Our previous studies revealed the presence of Li_2CO_3 on the surface of the as-synthesized $LiNiO_2$. This small decrease in cell polarization could be related to the decomposition of Li_2CO_3 surface species during the first cycle. Upon extended cycling, the paired oxidation and reduction peaks during the charge−discharge process progressively separated, the extent of which became large, in particular, in the high-voltage region (~4.2 V). The cell impedance rise over the extended cycles was also evidenced by an irreversible capacity when a lower current, C/10, was applied to the electrode after being cycled at C/3 for 25 cycles. Additionally, the oxidation peak at 4.18 V, related to H2-to-H3 transformation, was significantly reduced from the 10th to 45th cycle, suggesting that the H3 phase formation was suppressed. This could be attributed to the presence of Ni ions in Li layer, preventing Ni slab shifting and Li diffusion.[36] To test whether the bulk structural change was responsible for the capacity decay, we conducted ex situ SXRD at the end of charge and discharge states for the selected cycles to further investigate the phase evolution of $LiNiO_2$ over the extended cycles.

Ex situ SXRD patterns of the pristine and cycled $LiNiO_2$ electrodes were collected in the transmission mode; thus, the peaks from the Al current collector are present (black dash lines) in Figure 2. Due to the overlapping of Al peaks with the (102) and (104) peaks of $LiNiO_2$, our analysis was mainly focused on the most intense (003) diffraction peak with the assistance of other (*h*0*l*) diffraction peaks, which were sufficient to monitor the lattice changes and investigate the phase evolution. All the SXRD patterns were normalized to the intensity of the most-intense (003) diffraction peak for comparison. $LiNiO_2$ maintained good crystallinity and cation

DOI: 10.1021/acsami.6b11111
ACS Appl. Mater. Interfaces 2016, 8, 31677−31683

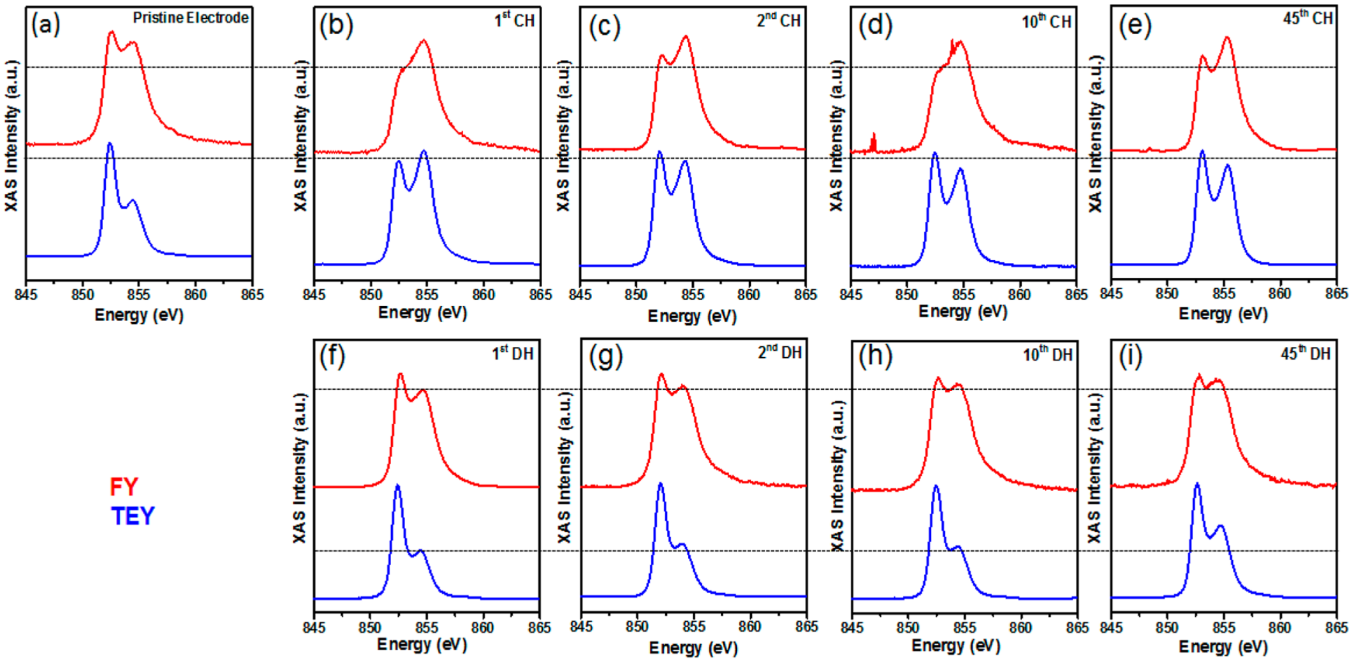

Figure 4. Soft XAS spectra of Ni L3-edge at: (a) pristine state, (b) 1st charge, (c) 2nd charge, (d) 10th charge, (e) 45th charge, (f) 1st discharge, (g) 2nd discharge, (h) 10th discharge, and (i) 45th discharge. The dash lines in the plots provide guidance for comparison of the Ni L3-edge between the 1st cycle and later cycles.

ordering after being formulated into an electrode. After the first charge, the (003) diffraction peak shifted to lower 2θ values and the ($h0l$) peaks shifted to higher 2θ values, suggesting the formation of a H2 phase with a larger c lattice parameter. At the end of the second charge, another set of diffraction peaks (green dash lines) appeared at slightly higher 2θ values than those associated with the H2 phase, indicating a contraction of the crystal lattice due to a H3 phase formation. Afterward, the H3 phase repeatedly occurred at the end of charge in subsequent cycles (cycle 10 and cycle 45). However, all H3 diffraction peaks became broadened and the intensity decreased remarkably, which is consistent with the significant reduction in the H3 oxidation peak shown on the dq/dV plot (Figure 1c). In addition to the structural change of the charged states, the pristine structure was not completely recovered after the first discharge. As shown in Figure 2b, the (003) peak slightly shifted to the lower angle region, compared to its pristine state, suggesting a small lattice expansion along the c direction, likely due to the irreversible structural changes that prevent the fully retaking of the Li ions. In subsequent cycles, the variations were fairly small, indicated by the similar peak positions and intensities in the SXRD patterns at discharged states.

The phase transformation is strongly related to the Li content in the cycled Li_xNiO_2 ($0 < x < 1$) electrode. The whole range was previously divided into four regions: (1) hexagonal H1 phase for $0 < x < 0.25$, (2) coexistence region of H1 and H2 phases for $0.25 < x < 0.55$, (3) second hexagonal H2 phase for $0.55 < x < 0.75$, and (4) coexisting H2 + H3 phase for $0.75 < x < 1$).[32] It is worth to point out that the Li contents for each region may vary. If we assume the starting $LiNiO_2$ electrode contained 1 mol Li per formula unit, about 0.887 Li was extracted from the lattice during the first charge; however, only the H2-phase formation was revealed. In addition, the oxidation and reduction peaks related to the H3 phase were observed in the dq/dV plot. Previous in situ XRD studies on fully charged Li_xNiO_2 electrode showed the H3-phase formation even for 0.82 Li removal.[30] In our case, decomposition of Li_2CO_3 surface species could contribute to the first charge capacity and account for the most irreversible capacity at 4.3 V cutoff. The extracted Li during the first charge was likely around 0.747 (1st cycle reversible Li), which was on the edge of the H2 + H3 coexistence region ($0.75 < x < 1$). During the second charge, the $Li_{1-x}NiO_2$ electrode with better electrolyte wetting, less polarization, or both resulted in a slightly greater Li extraction (therefore, a stable H3-phase formation). However, the discrepancy in the features related to H3-phase formation could result from the difference in electrochemical and ex situ SXRD measurements due to the possible relaxation of the H3 lattice during the ex situ SXRD experiment.

In parallel with the phase evolution tracked by SXRD, hard XAS was also performed at the Ni K-edge (8333 eV) to elucidate the charge-compensation mechanism and local environments around Ni ions (Figure 3). In the XANES (Figure 3a), the Ni edge shifted to higher energy after each selected charge state (dash lines) compared to the edge in the pristine electrode (black solid line), owing to the oxidation of Ni ions during the charge processes. Close examination of the edge positions on the derivative plots in Figure 3b revealed the highest Ni valence state at the end of the second charge (red dashed line), which is in accordance with the most prominent H3-phase formation (Figure 2a). It further confirmed that more Li ions were extracted during the second charge than the first charge. At the 10th and 45th cycle, the Ni edge at the charging states slightly moved to lower energy than that at the second charge. The discharge states (solid lines) upon cycling show a different trend in which a continuous shift to higher energy indicates less reduced Ni after repeated discharges. These two changes lead to the conclusion that the amount of electrons from Ni redox was getting smaller after cycling, and the decrease in Ni redox change resulted from both the charge and discharge states.

DOI: 10.1021/acsami.6b11111
ACS Appl. Mater. Interfaces 2016, 8, 31677−31683

To understand the local environment of Ni, we analyzed the Fourier-transformed (weighted) Ni K-edge extended X-ray absorption fine structure (EXAFS). In Figure 3c,d, the distinct peaks at 1.4 and 2.4 Å are assigned to the Ni−O and Ni−Ni interactions of the first and second coordination shells. Both Ni−O and Ni−Ni peaks shifted to lower R values after charging compared to those of the pristine state, indicating a contraction in the Ni−O and Ni−Ni interatomic distances due to the oxidation of Ni ions. However, the amplitude of these peaks varied at the end of charge for the selected cycles. The small and broad peak in the pristine state is due to the Jahn−Teller active Ni^{3+}.[49,50] During the repeated charges, the amplitude of these peaks increased and reached a maximum after the second charge then gradually decreased, suggesting a maximal degree of Ni oxidation after the second charge and a slight decrease after the charges in the later cycles. As opposed to the charge states, the Ni local environments were basically recovered after each discharge in the subsequent cycles (Figure 3d). The intensity of Ni−O (1.4 Å) and Ni−Ni (2.4 Å) shells tended to decrease at the 45th cycle; however, the intensity decrease at the discharged states was very small.

Soft XAS spectra were collected at various cycled states to investigate the variation of surface properties over the extended cycles (Figure 4). A pair of detection modes, total electron yield (TEY) and fluorescence yield (FY), were collected simultaneously on pristine and cycled electrodes. The different mean free paths of electrons and fluorescence photons in the samples enable a typical probing depth of 2−5 and ∼50 nm from the surface toward the bulk for TEY and FY mode, respectively. Valence-state changes for the Ni L-edge can be qualitatively obtained through the deconvolution of the Ni L3-edge into high-energy ($L3_{high}$) and low-energy ($L3_{low}$) states, where the ratio, $L3_{high}/L3_{low}$, is in a positive relationship with the Ni valence state. The FY and TEY modes of Ni L3-edge for electrodes at various states shown in Figure 4 are normalized with respect to the $L3_{low}$ feature. In the pristine state (Figure 4a), the $L3_{high}$-to-$L3_{low}$ ratio is smaller in TEY mode (blue) than that in FY mode (red), indicating a lower valence state of Ni ions at the surface compared to that in the bulk of the pristine electrode. After charge processes (Figure 4b−e), the $L3_{high}$-to-$L3_{low}$ ratio was systematically increased compared to that of the pristine electrode, owing to the Ni oxidation, although the Ni valence state at the surface was still lower than that in the bulk, as suggested by a smaller $L3_{high}$-to-$L3_{low}$ ratio in TEY mode. Interestingly, the $L3_{high}$-to-$L3_{low}$ ratios in TEY mode at charged states gradually decreased from the first to 45th cycle, indicating that the degree of Ni oxidation was reduced at the surface over the extended cycles. After the first discharge, the surface characteristics were similar to that in the pristine state. However, the $L3_{high}$-to-$L3_{low}$ ratio in TEY mode increased after the 10th discharge and further enlarged after the 45th discharge, revealing that the Ni reduction after the discharge over long-term cycling was not complete, i.e., the Ni redox reaction was not fully reversible at the surface. The trend of Ni oxidation change upon charging and discharging in FY mode is not as remarkable as that in TEY mode. This variation in FY mode is likely resulted by the experimental fluctuations due to the intrinsic origin of the fluorescent beam. Variation of Ni oxidation state in the bulk detected by hard XAS and at the surface by soft XAS showed that reversible Ni redox within each cycle was getting smaller both in the bulk and at the surface. This is direct evidence of the electronic structure changes that underpin the reversible capacity loss.

CONCLUSIONS

In summary, we investigated the phase evolution, charge compensation that occurred on Ni in the bulk and at the surface of $LiNiO_2$ over the extended cycles to understand the degradation mechanism. Our ex situ XRD experiments revealed the phase transition from the original hexagonal phase (H1) to another two hexagonal phases (H2 and H3) during the deintercalation processes, but the gradual loss of H3-phase features was revealed after the repeated charges. Moreover, ex situ XANES and EXAFS results showed more reduced Ni after the repeated charges and more oxidized Ni after the repeated discharges, suggesting a decrease in Ni redox activity over the extended cycles. Ex situ soft XAS analysis illustrated a similar trend in the Ni oxidation state change at the surface. Overall, the degradation in the crystal structure and Ni redox activity in the bulk and at the surface were responsible for the fast capacity fade of $LiNiO_2$. This aging mechanism of $LiNiO_2$ is of great importance in devising an optimization strategy for Ni-rich layered oxide cathodes in the next-generation Li-ion batteries.

AUTHOR INFORMATION

Corresponding Author

*E-mail: weitong@lbl.gov.

Author Contributions

The manuscript was written through contributions of all authors. All authors have given approval to the final version of the manuscript.

Notes

The authors declare no competing financial interest.

ACKNOWLEDGMENTS

This work was supported by the Assistant Secretary for Energy Efficiency and Renewable Energy, Office of Vehicle Technologies of the U.S. Department of Energy under contract no. DE-AC02-05CH11231. Synchrotron XRD and soft XAS work was carried out at the Stanford Synchrotron Radiation Lightsource, a Directorate of SLAC National Accelerator Laboratory and an Office of Science User Facility operated for the U.S. Department of Energy Office of Science by Stanford University. Use of the Stanford Synchrotron Radiation Lightsource, SLAC National Accelerator Laboratory, is supported by the U.S. Department of Energy, Office of Science, Office of Basic Energy Sciences under contract no. DE-AC02-76SF00515. The work at Brookhaven National Laboratory was supported by the U.S. Department of Energy, the Assistant Secretary for Energy Efficiency and Renewable Energy, Office of Vehicle Technologies under contract no. DE-SC0012704. W.T. greatly appreciates the fruitful discussion with Marca Doeff at Lawrence Berkeley National Laboratory.

REFERENCES

(1) Etacheri, V.; Marom, R.; Elazari, R.; Salitra, G.; Aurbach, D. Challenges in the Development of Advanced Li-Ion Batteries: a review. *Energy Environ. Sci.* **2011**, *4* (9), 3243−3262.
(2) Whittingham, M. S. Ultimate Limits to Intercalation Reactions for Lithium Batteries. *Chem. Rev.* **2014**, *114* (23), 11414−11443.
(3) Whittingham, M. S. Lithium Batteries and Cathode Materials. *Chem. Rev.* **2004**, *104* (10), 4271−4301.
(4) Nitta, N.; Wu, F.; Lee, J. T.; Yushin, G. Li-Ion Battery Materials: Present and Future. *Mater. Today* **2015**, *18* (5), 252−264.
(5) Choi, M. H.; Yoon, C. S.; Myung, S. T.; Lim, B. B.; Komaba, S.; Sun, Y. K. Effect of Lithium in Transition Metal Layers of Ni-Rich

Cathode Materials on Electrochemical Properties. *J. Electrochem. Soc.* **2015**, *162* (12), A2313−A2318.
(6) Hwang, B. J.; Tsai, Y. W.; Chen, C. H.; Santhanam, R. Influence of Mn Content on the Morphology and Electrochemical Performance of LiNi1-x-yCoxMnyO2 Cathode Materials. *J. Mater. Chem.* **2003**, *13* (8), 1962−1968.
(7) Shi, J.-L.; Zhang, J.-N.; He, M.; Zhang, X.-D.; Yin, Y.-X.; Li, H.; Guo, Y.-G.; Gu, L.; Wan, L.-J. Mitigating Voltage Decay of Li-Rich Cathode Material via Increasing Ni Content for Lithium-Ion Batteries. *ACS Appl. Mater. Interfaces* **2016**, *8* (31), 20138−20146.
(8) Qing, R.-P.; Shi, J.-L.; Xiao, D.-D.; Zhang, X.-D.; Yin, Y.-X.; Zhai, Y.-B.; Gu, L.; Guo, Y.-G. Enhancing the Kinetics of Li-Rich Cathode Materials through the Pinning Effects of Gradient Surface Na+ Doping. *Adv. Energy Mater.* **2016**, *6* (6).10.1002/aenm.201670035
(9) Wu, L.; Nam, K.-W.; Wang, X.; Zhou, Y.; Zheng, J.-C.; Yang, X.-Q.; Zhu, Y. Structural Origin of Overcharge-Induced Thermal Instability of Ni-Containing Layered-Cathodes for High-Energy-Density Lithium Batteries. *Chem. Mater.* **2011**, *23* (17), 3953−3960.
(10) Kuriyama, H.; Saruwatari, H.; Satake, H.; Shima, A.; Uesugi, F.; Tanaka, H.; Ushirogouchi, T. Observation of Anisotropic Microstructural Changes during Cycling in LiNi0.5Co0.2Mn0.3O2 Cathode Material. *J. Power Sources* **2015**, *275*, 99−105.
(11) Lee, Y. M.; Nam, K. M.; Hwang, E. H.; Kwon, Y. G.; Kang, D. H.; Kim, S. S.; Song, S. W. Interfacial Origin of Performance Improvement and Fade for 4.6 V LiNi0.5Co0.2Mn0.3O2 Battery Cathodes. *J. Phys. Chem. C* **2014**, *118* (20), 10631−10639.
(12) Lin, F.; Nordlund, D.; Markus, I. M.; Weng, T.-C.; Xin, H. L.; Doeff, M. M. Profiling the Nanoscale Gradient in Stoichiometric Layered Cathode Particles for Lithium-Ion Batteries. *Energy Environ. Sci.* **2014**, *7* (9), 3077−3085.
(13) Lin, F.; Markus, I. M.; Nordlund, D.; Weng, T.-C.; Asta, M. D.; Xin, H. L.; Doeff, M. M. Surface Reconstruction and Chemical Evolution of Stoichiometric Layered Cathode Materials for Lithium-Ion Batteries. *Nat. Commun.* **2014**, *5*, 3529.
(14) Hwang, S.; Kim, S. M.; Bak, S.-M.; Cho, B.-W.; Chung, K. Y.; Lee, J. Y.; Chang, W.; Stach, E. A. Investigating Local Degradation and Thermal Stability of Charged Nickel-Based Cathode Materials through Real-Time Electron Microscopy. *ACS Appl. Mater. Interfaces* **2014**, *6* (17), 15140−15147.
(15) Hwang, S.; Chang, W.; Kim, S. M.; Su, D.; Kim, D. H.; Lee, J. Y.; Chung, K. Y.; Stach, E. A. Investigation of Changes in the Surface Structure of LixNi0.8Co0.15Al0.05O2 Cathode Materials Induced by the Initial Charge. *Chem. Mater.* **2014**, *26* (2), 1084−1092.
(16) Bak, S.-M.; Nam, K.-W.; Chang, W.; Yu, X.; Hu, E.; Hwang, S.; Stach, E. A.; Kim, K.-B.; Chung, K. Y.; Yang, X.-Q. Correlating Structural Changes and Gas Evolution during the Thermal Decomposition of Charged LixNi0.8Co0.15Al0.05O2 Cathode Materials. *Chem. Mater.* **2013**, *25* (3), 337−351.
(17) Noh, H.-J.; Youn, S.; Yoon, C. S.; Sun, Y.-K. Comparison of the Structural and Electrochemical Properties of Layered Li[NixCoyMnz]-O2 (x = 1/3, 0.5, 0.6, 0.7, 0.8 and 0.85) Cathode Material for Lithium-Ion Batteries. *J. Power Sources* **2013**, *233*, 121−130.
(18) Bang, H. J.; Joachin, H.; Yang, H.; Amine, K.; Prakash, J. Contribution of the Structural Changes of LiNi0.8Co0.15Al0.05O2 Cathodes on the Exothermic Reactions in Li-Ion Cells. *J. Electrochem. Soc.* **2006**, *153* (4), A731−A737.
(19) Bak, S. M.; Hu, E. Y.; Zhou, Y. N.; Yu, X. Q.; Senanayake, S. D.; Cho, S. J.; Kim, K. B.; Chung, K. Y.; Yang, X. Q.; Nam, K. W. Structural Changes and Thermal Stability of Charged LiNixMnyCo-zO2 Cathode Materials Studied by Combined In Situ Time-Resolved XRD and Mass Spectroscopy. *ACS Appl. Mater. Interfaces* **2014**, *6* (24), 22594−22601.
(20) Eom, J.; Kim, M. G.; Cho, J. Storage Characteristics of LiNi0.8Co0.1 + x Mn0.1 − x O2 (x = 0, 0.03, and 0.06) Cathode Materials for Lithium Batteries. *J. Electrochem. Soc.* **2008**, *155* (3), A239−A245.
(21) Muto, S.; Sasano, Y.; Tatsumi, K.; Sasaki, T.; Horibuchi, K.; Takeuchi, Y.; Ukyo, Y. Capacity-Fading Mechanisms of LiNiO2-Based Lithium-Ion Batteries: II. Diagnostic Analysis by Electron Microscopy and Spectroscopy. *J. Electrochem. Soc.* **2009**, *156* (5), A371−A377.
(22) Sasaki, T.; Nonaka, T.; Oka, H.; Okuda, C.; Itou, Y.; Kondo, Y.; Takeuchi, Y.; Ukyo, Y.; Tatsumi, K.; Muto, S. Capacity-Fading Mechanisms of LiNiO2-Based Lithium-Ion Batteries: I. Analysis by Electrochemical and Spectroscopic Examination. *J. Electrochem. Soc.* **2009**, *156* (4), A289−A293.
(23) Muto, S.; Tatsumi, K.; Sasaki, T.; Kondo, H.; Ohsuna, T.; Horibuchi, K.; Takeuchi, Y. Mapping of Heterogeneous Chemical States of Lithium in a LiNiO2-Based Active Material by Electron Energy-Loss Spectroscopy. *Electrochem. Solid-State Lett.* **2010**, *13* (8), A115−A117.
(24) Kojima, Y.; Muto, S.; Tatsumi, K.; Kondo, H.; Oka, H.; Horibuchi, K.; Ukyo, Y. Degradation Analysis of a Ni-Based Layered Positive-Electrode Active Material Cycled at elevated temperatures studied by scanning transmission electron microscopy and electron Energy-Loss Spectroscopy. *J. Power Sources* **2011**, *196* (18), 7721−7727.
(25) Konishi, H.; Yoshikawa, M.; Hirano, T. The Effect of Thermal Stability for High-Ni-Content Layer-Structured Cathode Materials, LiNi0.8Mn0.1−xCo0.1MoxO2 (x = 0, 0.02, 0.04). *J. Power Sources* **2013**, *244*, 23−28.
(26) Xiong, X.; Wang, Z.; Yue, P.; Guo, H.; Wu, F.; Wang, J.; Li, X. Washing Effects on Electrochemical Performance and Storage Characteristics of LiNi0.8Co0.1Mn0.1O2 as Cathode Material for Lithium-Ion Batteries. *J. Power Sources* **2013**, *222*, 318−325.
(27) Jung, S.-K.; Gwon, H.; Hong, J.; Park, K.-Y.; Seo, D.-H.; Kim, H.; Hyun, J.; Yang, W.; Kang, K. Understanding the Degradation Mechanisms of LiNi0.5Co0.2Mn0.3O2 Cathode Material in Lithium Ion Batteries. *Adv. Energy Mater.* **2014**, *4* (1).130078710.1002/aenm.201300787
(28) Zheng, J. M.; Kan, W. H.; Manthiram, A. Role of Mn Content on the Electrochemical Properties of Nickel-Rich Layered LiNi0.8-xCo0.1Mn0.1+xO2 (0.0 $\leq x \leq$ 0.08) Cathodes for Lithium-Ion Batteries. *ACS Appl. Mater. Interfaces* **2015**, *7* (12), 6926−6934.
(29) Yan, P. F.; Zheng, J. M.; Lv, D. P.; Wei, Y.; Zheng, J. X.; Wang, Z. G.; Kuppan, S.; Yu, J. G.; Luo, L. L.; Edwards, D.; Olszta, M.; Amine, K.; Liu, J.; Xiao, J.; Pan, F.; Chen, G. Y.; Zhang, J. G.; Wang, C. M. Atomic-Resolution Visualization of Distinctive Chemical Mixing Behavior of Ni, Co, and Mn with Li in Layered Lithium Transition-Metal Oxide Cathode Materials. *Chem. Mater.* **2015**, *27* (15), 5393−5401.
(30) Li, W.; Reimers, J. N.; Dahn, J. R. In-Situ X-ray-Diffraction and Electrochemical Studies of Li1-xNiO2. *Solid State Ionics* **1993**, *67* (1−2), 123−130.
(31) Dokko, K.; Nishizawa, M.; Horikoshi, S.; Itoh, T.; Mohamedi, M.; Uchida, I. In Situ Observation of LiNiO2 Single-Particle Fracture during Li-Ion Extraction and Insertion. *Electrochem. Solid State Lett.* **2000**, *3* (3), 125−127.
(32) Yang, X. Q.; Sun, X.; McBreen, J. New Findings on the Phase Transitions in Li1-xNiO2: In Situ Synchrotron X-ray Diffraction Studies. *Electrochem. Commun.* **1999**, *1* (6), 227−232.
(33) Guilmard, M.; Croguennec, L.; Denux, D.; Delmas, C. Thermal Stability of Lithium Nickel Oxide Derivatives. Part I: LixNi1.02O2 and LixNi0.89Al0.16O2 (x = 0.50 and 0.30). *Chem. Mater.* **2003**, *15* (23), 4476−4483.
(34) Delmas, C.; Ménétrier, M.; Croguennec, L.; Levasseur, S.; Pérès, J. P.; Pouillerie, C.; Prado, G.; Fournès, L.; Weill, F. Lithium Batteries: a New Tool in Solid State Chemistry. *Int. J. Inorg. Mater.* **1999**, *1* (1), 11−19.
(35) Arai, H.; Okada, S.; Ohtsuka, H.; Ichimura, M.; Yamaki, J. Characterization and Cathode Performance of Li1 − xNi1 + xO2 Prepared with the Excess Lithium Method. *Solid State Ionics* **1995**, *80* (3−4), 261−269.
(36) Ohzuku, T.; Ueda, A.; Nagayama, M. Electrochemistry and Structural Chemistry of LiNiO2 ($R\bar{3}m$) for 4 V Secondary Lithium Cells. *J. Electrochem. Soc.* **1993**, *140* (7), 1862−1870.
(37) Chang, K.; Hallstedt, B.; Music, D. Thermodynamic Description of the LiNiO2−NiO2 Pseudo-Binary System and Extrapolation to the

Li(Co,Ni)O2−(Co,Ni)O2 System. *CALPHAD: Comput. Coupling Phase Diagrams Thermochem.* **2012**, *37* (0), 100−107.
(38) Li, J.; Downie, L. E.; Ma, L.; Qiu, W.; Dahn, J. R. Study of the Failure Mechanisms of LiNi0.8Mn0.1Co0.1O2 Cathode Material for Lithium Ion Batteries. *J. Electrochem. Soc.* **2015**, *162* (7), A1401−A1408.
(39) Li, J.; Shunmugasundaram, R.; Doig, R.; Dahn, J. R. In Situ X-ray Diffraction Study of Layered Li−Ni−Mn−Co Oxides: Effect of Particle Size and Structural Stability of Core−Shell Materials. *Chem. Mater.* **2016**, *28* (1), 162−171.
(40) Xie, H.; Du, K.; Hu, G.; Peng, Z.; Cao, Y. The Role of Sodium in LiNi0.8Co0.15Al0.05O2 Cathode Material and Its Electrochemical Behaviors. *J. Phys. Chem. C* **2016**, *120* (6), 3235−3241.
(41) Yang, J.; Xia, Y. Suppressing the Phase Transition of the Layered Ni-Rich Oxide Cathode during High-Voltage Cycling by Introducing Low-Content Li2MnO3. *ACS Appl. Mater. Interfaces* **2016**, *8* (2), 1297−1308.
(42) Dokko, K.; Nishizawa, M.; Horikoshi, S.; Itoh, T.; Mohamedi, M.; Uchida, I. In Situ Observation of LiNiO2 Single-Particle Fracture during Li-Ion Extraction and Insertion. *Electrochem. Solid-State Lett.* **2000**, *3* (3), 125−127.
(43) Nakai, I.; Takahashi, K.; Shiraishi, Y.; Nakagome, T.; Izumi, F.; Ishii, Y.; Nishikawa, F.; Konishi, T. X-ray Absorption Fine Structure and Neutron Diffraction Analyses of De-Intercalation Behavior in the LiCoO2 and LiNiO2 Systems. *J. Power Sources* **1997**, *68* (2), 536−539.
(44) Nakai, I.; Takahashi, K.; Shiraishi, Y.; Nakagome, T.; Nishikawa, F. Study of the Jahn-Teller Distortion in LiNiO2, a Cathode Material in a Rechargeable Lithium Battery, by In Situ X-ray Absorption Fine Structure Analysis. *J. Solid State Chem.* **1998**, *140* (1), 145−148.
(45) Mansour, A. N.; Yang, X. Q.; Sun, X.; McBreen, J.; Croguennec, L.; Delmas, C. In Situ X-ray Absorption Spectroscopy Study of Li(1-z)Ni(1+z)O2 ($z \leq 0.02$) Cathode Material. *J. Electrochem. Soc.* **2000**, *147* (6), 2104−2109.
(46) Mansour, A. N.; McBreen, J.; Melendres, C. A. An In Situ X-ray Absorption Spectroscopic Study of Charged Li((1-z))Ni((1+z))O2 Cathode Material. *J. Electrochem. Soc.* **1999**, *146* (8), 2799−2809.
(47) Xu, J.; Lin, F.; Nordlund, D.; Crumlin, E. J.; Wang, F.; Bai, J.; Doeff, M. M.; Tong, W. Elucidation of the Surface Characteristics and Electrochemistry of High-Performance LiNiO2. *Chem. Commun.* **2016**, *52* (22), 4239−4242.
(48) Li, W.; Reimers, J. N.; Dahn, J. R. In Situ X-ray Diffraction and Electrochemical Studies of Li1−xNiO2. *Solid State Ionics* **1993**, *67* (1−2), 123−130.
(49) Balasubramanian, M.; Sun, X.; Yang, X. Q.; McBreen, J. In Situ X-ray Absorption Studies of a High-Rate LiNi0.85Co0.15O2 Cathode Material. *J. Electrochem. Soc.* **2000**, *147* (8), 2903−2909.
(50) Balasubramanian, M.; Sun, X.; Yang, X. Q.; McBreen, J. In Situ X-ray Diffraction and X-ray Absorption Studies of High-Rate Lithium-Ion Batteries. *J. Power Sources* **2001**, *92* (1−2), 1−8.

DOI: 10.1021/acsami.6b11111
ACS Appl. Mater. Interfaces 2016, 8, 31677−31683